On the seasonal cycle of the statistical properties of Sea Surface Temperature

J. Isern-Fontanet[1,2], X. Capet[3], A. Turiel[1,2], E. Olmedo[1,2], C. González-Haro[1,2]

[1]Institut de Ciències del Mar (CSIC), Barcelona, EU
[2]Barcelona Expert Centre in Remote Sensing, Barcelona, EU
[3]LOCEAN, Paris, EU

Key Points:

- The intensity of SST fronts is quantified using singularity exponents, which measure the continuity of the field
- Anomalous scaling of SST structure functions is correlated to the the intensity of the strongest fronts
- The variability of the strongest fronts depends on the seasonal variability of the coastal upwelling in the area of study

Corresponding author: J. Isern-Fontanet, `jisern@icm.csic.es`

Abstract

The contribution of ocean fronts to the properties and temporal evolution of Sea Surface Temperature (SST) structure functions have been investigated using a numerical model of the California Current system. First, the intensity of fronts have been quantified by using singularity exponents. Then, leaning on the multifractal theory of turbulence, we show that the departure of the scaling of the structure functions from a straight line, known as anomalous scaling, depends on the intensity of the strongest fronts. These fronts, at their turn, are closely related to the seasonal change of intensity of the coastal upwelling characteristics of this area. Our study points to the need to correctly reproduce the intensity of the strongest fronts and, consequently, properly model processes such as coastal upwelling in order to reproduce SST statistics in ocean models.

Plain Language Summary

Forecasting the evolution of Earth Climate requires to predict the evolution of the statistical characteristics of essential climate variables such as the Sea Surface Temperature. In this study, it has been found that some of such statistical properties depend on the intensity of the strongest fronts in the ocean. This implies that those ocean, or climate, models that fail to correctly predict their intensity won't be able to correctly reproduce the statistical characteristics of key variables such as temperature. The area analyzed in this study is the California Current system, where the strongest fronts are modulated by the seasonal evolution of the upwelling. Therefore, our results imply that such a system has to be correctly modeled in order to properly reproduce the statistics of ocean temperatures.

1 Introduction

Sea Surface Temperature (SST) is a fundamental variable of the Earth climate system due to its role in regulating climate and weather (Deser et al., 2010) and its dynamical connection to ocean currents (Isern-Fontanet et al., 2014). Moreover, the availability of long time series of global high resolution satellite measurements of SST (Merchant et al., 2019) makes it well suited for addressing a wide range of problems such as monitoring the Climate Change (Gulev et al., 2021); retrieving ocean currents (Isern-Fontanet et al., 2017); or calibrating and validating ocean and climate models (Skákala et al., 2019). It is, therefore, of major importance to understand how ocean processes contribute to

SST statistics to exploit such a wealth of data and get insight into the functioning of the ocean and climate.

A prominent feature of SST is the presence of fronts, which are known to be sinks of energy (D'Asaro et al., 2011; Isern-Fontanet & Turiel, 2021) and significantly contribute to the vertical transport of nutrients and, thus, to primary production (Mahadevan, 2016). The variability of the characteristics of fronts, such as the density of fronts or their intensity, are expected to be mirrored by the variability of some SST statistics. A popular approach is based on the spectral slope of SST because it can be connected to theories of turbulence. Nevertheless, they provide an incomplete framework, if only because different theories may predict the same slope (Callies & Ferrari, 2013) and the underlying turbulence regime may not change in spite of the seasonal changes in the properties of fronts.

The structure functions of a turbulent variable, i.e. the moments of the differences between two points, are also at the core of theories of turbulence (Pope, 2000) and extend the information provided by spectral slopes (Yu et al., 2017; Sukhatme et al., 2020). Moreover, the anomalous scaling of the power laws deduced from the structure functions, i.e. its deviation from a straight line, can be related to the geometry of gradients making use of the multifractal framework (Isern-Fontanet & Turiel, 2021). The relevance of this approach has already been demonstrated in the oceanic context. (Isern-Fontanet et al., 2007) and it has been used to develop metrics for model validation (Ivanov et al., 2009; Skákala et al., 2016), although it has not been yet exploited to investigate the contribution of fronts to SST statistics.

Here, we introduce a metric to measure the intensity of SST fronts in numerical simulations of the California Current System (Capet, McWilliams, et al., 2008), which is dominated by cross-shore gradients generated by the coastal upwelling (Chenillat et al., 2018). This metric is then connected to the scaling of the structure functions using the multifractal framework (Frisch, 1995) and used to investigate how the temporal variability of front intensity contribute to the variability of anomalous scaling and spectral slopes. The paper is organized as follows: section 2 puts the multifractal theory of turbulence in the context of oceanography; section 3 describes the numerical simulations and the algorithms used for this study; sections 4 and 5 describe results and discuss them, respectively; and section 6 list the conclusions.

2 Theoretical framework

Coarse-grained Sea Surface Temperature (SST) gradients are built by filtering the module of the thermal gradient as

$$\overline{|\nabla T|}_\ell(\vec{x}) \equiv \int_{\mathbf{R}^d} \ell^{-d} G(\ell^{-1}\vec{x}) |\nabla T|(\vec{x}+\vec{x}')d\vec{x}', \quad (1)$$

where $d = 2$ is the geometrical dimension; ℓ is the scale of the filter; $G(\vec{x})$ is a normalized positive function that decays fast to zero as $|\vec{x}| \to \infty$; $T(\vec{x})$ is the SST and $\nabla = (\partial_x, \partial_y)$. These SST gradients are known to possess a range of scaling exponents $h(\vec{x})$ that verify

$$\overline{|\nabla T|}_\ell(\vec{x}) \sim \left(\frac{\ell}{\ell_0}\right)^{h(\vec{x})} \quad (2)$$

as $\ell/\ell_0 \to 0$, where ℓ_0 is the integral scale of the flow (Isern-Fontanet et al., 2007). The scaling exponents $h(\vec{x})$, known as singularity or Hölder exponents, quantify the degree of continuity of SST. Indeed, if $h(\vec{x}) \in (n, n{+}1)$ with n being a positive integer, $\overline{|\nabla T|}_\ell(\vec{x})$ is derivable n times but not $n{+}1$ (Arneodo et al., 1995). Consequently, we propose the use of singularity exponents as a proxy measure for the intensity of fronts, on the basis that the strongest fronts are those with the most marked singularity, hence also those with the smallest singularity exponents. .

The domain of the turbulent flow can be, then, divided into subsets according to their singularity exponent. This gives rise to the singularity spectrum, a concave function of h defined as

$$D(h') \equiv d_F\left(\{\vec{x}|h(\vec{x}) = h'\}\right), \quad (3)$$

where $d_F(A)$ is the fractal dimension of set A. It follows that, the singularity spectrum $D(h)$ characterizes the 'volume' occupied by fronts with intensity h. Moreover, the singularity spectrum $D(h)$ provides information about the statistical properties of SST. Indeed, the scaling properties of the moments of SST gradients are defined by a continuous function $\tau(p)$ of the moment order p

$$\langle \overline{|\nabla T|}_\ell^p \rangle \sim \left(\frac{\ell}{\ell_0}\right)^{\tau(p)}, \quad (4)$$

which is related to the singularity spectrum by a Legendre transform pair

$$\tau(p) = ph + d - D(h), \quad \text{with} \quad p = \frac{dD}{dh} \quad (5)$$

and

$$D(h) = ph + d - \tau(p), \quad \text{with} \quad h = \frac{d\tau}{dp}, \quad (6)$$

as shown by Parisi and Frisch (1985). It's worth mentioning that equation 4 implies that the Probability Density Functions (PDF) of thermal gradients are dependent on the analysis scale ℓ, which is a signature of intermittency (Frisch, 1995). As a consequence, care must be taken when analysing PDF and kurtosis and when comparing PDF from data with different resolutions.

The singularity spectrum can also be related to the scaling of the structure functions of temperature, which are defined as

$$S_p(\ell) \equiv \langle |T_s(\vec{x}+\vec{\ell}) - T_s(\vec{x})|^p \rangle \tag{7}$$

and scale according to the continuous function $\zeta(p)$, i.e.

$$S_p(\ell) \sim \left(\frac{\ell}{\ell_0}\right)^{\zeta(p)}. \tag{8}$$

Using that, at small scales, $|T_s(\vec{x}+\vec{\ell}) - T_s(\vec{x})| \sim \ell|\nabla T|$ it follows that,

$$\frac{1}{\ell_0^p}\langle |T_s(\vec{x}+\vec{\ell}) - T_s(\vec{x})|^p \rangle \sim \left(\frac{\ell}{\ell_0}\right)^p \langle \overline{|\nabla T|}_\ell^p \rangle \sim \left(\frac{\ell}{\ell_0}\right)^p \left(\frac{\ell}{\ell_0}\right)^{\tau(p)} \sim \frac{1}{\ell_0^p}\left(\frac{\ell}{\ell_0}\right)^{\zeta(p)}, \tag{9}$$

with ℓ_0 being a constant, and, consequently, both scaling functions are related by

$$\zeta(p) = p + \tau(p). \tag{10}$$

Recall that, the scaling of the structure function of order $p = 2$ gives the spectral slope of SST,

$$E(k) \propto k^{-\zeta(2)-1} = k^{-\tau(2)-3}, \tag{11}$$

where $E(k)$ is the energy spectrum and k the wavenumber (Frisch, 1995).

Guided by the recent work of Isern-Fontanet and Turiel (2021), here, we focus on two properties of the singularity spectrum: the most singular exponent h_∞,

$$h_\infty \equiv \min(h), \tag{12}$$

which is a measure of the intensity of the strongest fronts; and the width of the singularity spectrum defined as

$$\Delta h^- \equiv h_d - h_\infty, \tag{13}$$

where h_d is the mode. This quantity corresponds to the difference of slopes of $\zeta(p)$ between the origin ($p = 0$) and large orders ($p \to \infty$). Indeed, using equation (6) and equation (10), it can be seen that

$$\left.\frac{d\zeta}{dp}\right|_{p=0} - \left.\frac{d\zeta}{dp}\right|_{p\to\infty} = \left.\frac{d\tau}{dp}\right|_{p=0} - \left.\frac{d\tau}{dp}\right|_{p\to\infty} = h_d - h_\infty = \Delta h^-. \tag{14}$$

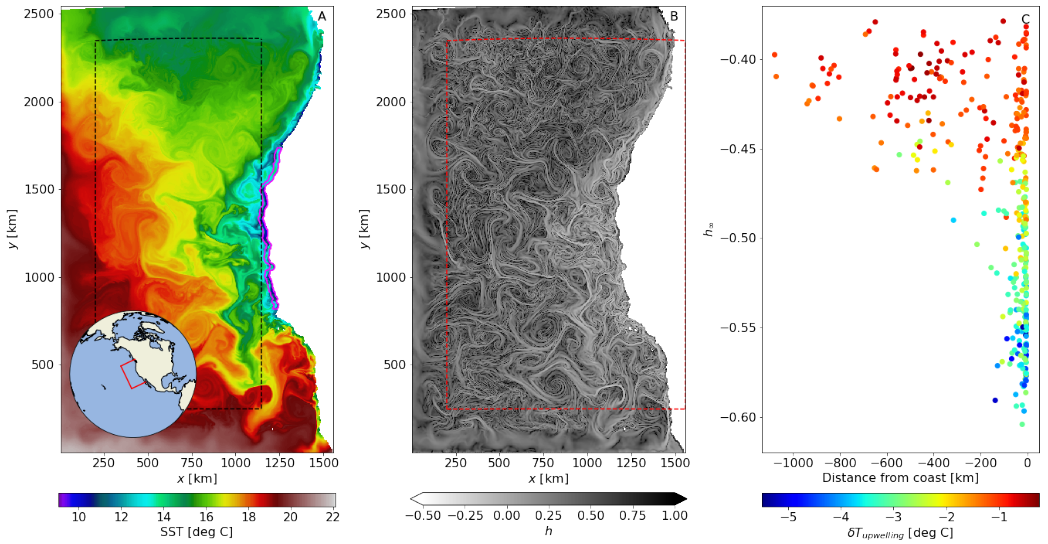

Figure 1. A: Example of instantaneous SST corresponding to July 10th of the first year analyzed (t=20 days) with the area used to compute Fourier spectra (black, dashed) and $\delta T_{upwelling}$ (purple, solid). The inset globe shows the geographical limits of the numerical simulations. B: singularity exponents for the SST image with the area used to compute singularity spectra (red, dashed). C: distance from coast of of the h_∞ observed for the whole analyzed period with the color corresponding to $\delta T_{upwelling}$.

Therefore, the anomalous scaling, i.e. the departure from a straight line, increases with growing Δh^-.

3 Data and procedures

SST fields were taken from numerical simulations of the circulation in the California Current System (see figure 1A) generated with the ROMS oceanic model (Shchepetkin & McWilliams, 2005). The model was configured with a horizontal resolution of ~ 2.5 km (1025×625 grid points) and 32 vertical levels with higher resolution in the upper layers. The boundary and initial conditions, as well as the forcing at the air-sea interface (wind stress, heat and freshwater fluxes) were derived from climatologies as in Capet, Colas, et al. (2008). Singularity analysis was applied to snapshots of SST taken every two days of simulation spanning a period of two years.

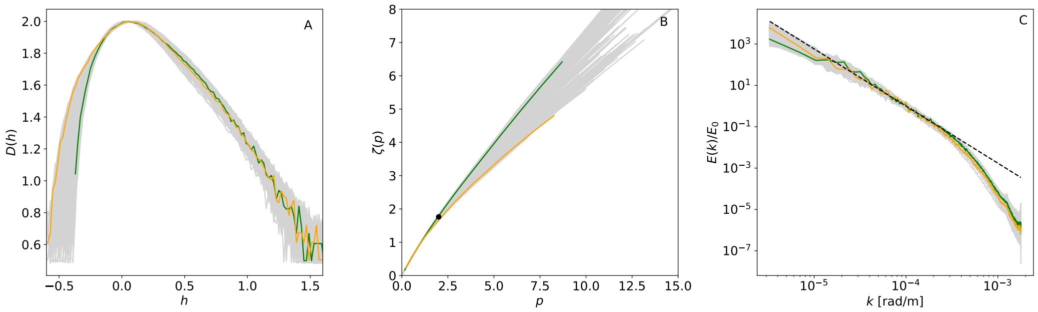

Figure 2. A: Singularity spectra $D(h)$. B: scaling of the structure functions of temperature $\zeta(p)$ derived from the singularity spectra. The black dot corresponds to $\langle\zeta(2)\rangle$. C: normalized Fourier spectra. The black dashed line has a slope given by $-\langle\zeta(2)\rangle - 1$. Energy spectra are normalized by $E_0 \equiv E(k_0)$, where $k = 10^{-4}$ rad/m. Grey lines correspond to the observations for the full period, while orange and green lines correspond the examples of two particular days: March 4th (green, $t = 246$ days) and August 23rd (orange, $t = 418$ days) of the second year.

Although very appealing, equation (2) can not be used directly to compute singularity exponents due to long-range correlations and discretization effects (Turiel et al., 2008). To avoid these difficulties, we used the method proposed by Pont et al. (2013) to compute singularity exponents (see figure 1B). Then, the singularity spectrum of each snapshot of SST was computed within the domain of analysis (see red rectangle in figure 1B) using the histogram method

$$D(h_i) \approx d - \frac{\log N_i - \log N_{max}}{\log(\ell/\ell_0)}, \tag{15}$$

where N_i is the number of grid cells having a singularity exponent in the range $[h_i - \frac{\delta h}{2}, h_i + \frac{\delta h}{2})$, N_{max} the number of valid ocean grid cells in the analysis domain, and $\ell/\ell_0 = (\sum_i N_i)^{\frac{1}{d}}$ (Turiel et al., 2006). The grid points surrounding the land mask were removed to avoid spurious values due to the land-sea transition and we used $d = 2$ and $\delta h = 0.02$ in the range from $h = -1$ to $h = 3$ for computing $D(h)$. Translational invariance was imposed to each singularity spectrum to correct for any shift that may exist in the singularity exponents (Isern-Fontanet & Turiel, 2021). This invariant condition consists in imposing that the $\langle\overline{|\nabla T|_\ell}\rangle$ does not depends on ℓ, i.e. $\tau(1) \equiv 0$. Finally, the mode h_d was estimated by locally adjusting a parabola around the maximum of $D(h)$ and, then, analytically calculating its maximum.

The function $\zeta(p)$ was derived from the instantaneous $D(h)$ by first applying the Legendre transform equations (5) and, then, equation (10). To reduce the spurious oscillations due to noise, we used a similar approach to the computation of h_d, i.e. the Legendre transform was obtained by locally fitting a second order polynomial to the surroundings of each value of $D(h_i)$ and, then, analytically inverting it. On the contrary, the SST spectrum was computed independently from $D(h)$ using SST anomalies in the black box shown in figure 1A, i.e.

$$\delta T(\vec{x},t) = T(\vec{x},t) - \tilde{T}(\vec{x},t), \tag{16}$$

where $\tilde{T}(\vec{x},t) \equiv a_x(t)x + a_y(t)y + a_{xy}(t)xy + a_0(t)$ was estimated by least-squares fitting to SST in the whole domain. With the aim of having a simple measure of the intensity of the coastal upwelling, the temperature anomaly associated to it was defined as the mean temperature anomaly close to the coast, i.e.

$$\delta T_{upwelling}(t) \equiv \langle \delta T(\vec{x},t) \rangle_{upwelling}. \tag{17}$$

This area was taken as the area between the coast and 10 grid points seawards ($\sim$ 25 km) and between y =810 km and y =1720 km, which corresponds the purple area marked in figure 1A.

4 Results

Figure 1B unveils the complex structure of thermal fronts observable in a snapshot of SST, with the most intense fronts, bright lines in the figure, being those with smaller singularity exponents. The intensity of fronts has some spatial variability. On one side, the areas with blurred fronts found in the North, West and South limits of the domain are due to the low-resolution information imposed at the model open boundary conditions. On the other, the intensity of fronts tend to be higher within the area strongly influenced by coastal upwelling (the area within [600 km, 1150 km]$\times$[700 km, 1700 km] approximately). Moreover, results shown in figure 1C reveal that the smallest values of h_∞ are concentrated close to the coast and correspond to large values of $|\delta T_{upwelling}|$, while larger values of h_∞ can be found away from the coast for and correspond to small values of $|\delta T_{upwelling}|$.

Singularity spectra $D(h)$ are asymmetric functions of h, whose properties change over time as revealed by figure 2A. Indeed, the value of h_∞ ranges between -0.6 and -0.35 for the two years of simulation and the width Δh^- between 0.4 and 0.7. The changes in the width of $D(h)$ are related to changes in the anomalous scaling of the structure functions (figure 2B) as expected from equation 14. Such changes are more pronounced for moments larger than $p = 2$ (which provides the spectral slope of SST; equation 11). Moreover, the slope of the instantaneous spectra of SST for $k < 10^{-4}$ rad/m , which has been computed independently, is close to the value given by the average $\langle\zeta(2)\rangle$ computed from the singularity spectra $D(h)$ (figure 2C). The observed spectral slope is somewhat steeper than k^{-2}, in contrast to Capet, McWilliams, et al. (2008). A shallower spectral slope can be recovered by reducing the spectral analysis to the area dominated by the upwelling, where fronts are stronger and more energy is present at the smaller resolved scales (not shown).

The two properties analyzed in this study, h_∞ and Δh^- are not independent but are strongly correlated with a linear correlation of -0.98 and a slope between them of -1.13 (figure 3A). A closer look, however, shows that the snapshots with $h_\infty < -0.5$ have weaker slopes between h_∞ and Δh^- (-1.11) and a tendency to have larger values of $|\delta T_{upwelling}|$ (3.56 deg C on average) than snapshots with $h_\infty > -0.5$ (-1.14 and 1.66 deg C on average, respectively). Besides, the temporal evolution of h_∞ follows a seasonal cycle (figure 3B), which has associated a seasonal variation of the width of the singularity spectrum of SST gradients and, thus, a seasonal variation of the anomalous scaling of the structure functions of temperature. Moreover, the close relation between the spatial location of h_∞ and $\delta T_{upwelling}$ shown in figure 1C suggests a strong relationship between them, which is confirmed statistically: the Pearson correlation coefficient between the temporal evolution of h_∞ and $\delta T_{upwelling}$ (figure 3B) is 0.87.

5 Discussion

In this study we have proposed, for the first time, to measure the intensity of fronts in SST using the singularity exponents of thermal gradients. Singularity exponents characterise the scaling at small scales, are independent of the gradient magnitude and measure the degree of continuity of the field. Moreover, singularity exponents have the advantage over other popular approaches for detecting fronts (Chang & Cornillon, 2015; Kirches et al., 2016) that they can be easily connected to statistical quantities that are central to turbulence theories. Indeed, the singularity spectrum, which gives the fractal dimension of those points with the same exponents, emerges as a fundamental property of the ocean providing the link between anomalous scaling and the intensity of fronts.

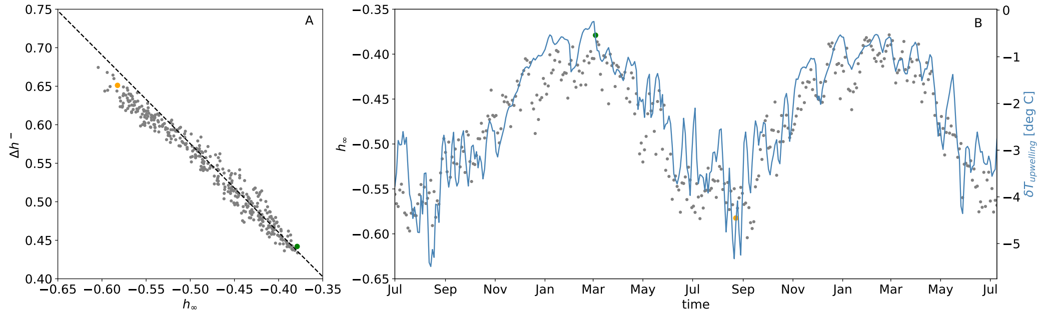

Figure 3. A: Scatter plot between h_∞ and Δh^-. The black line corresponds to a slope of -1.13. B: temporal evolution of h_∞ and $\delta T_{upwelling}$. Grey points correspond to the observations for the full period, while orange and green points correspond to the examples of two particular days: March 4th (green, t=246 days) and August 23rd (orange, t=418 days) of the second year.

Here, we have exploited this relationship to understand the seasonal variability of the scaling of the structure functions in the California Current System.

Two main results have been reported in this study. First, there is a seasonal variability in the value of the most singular (the smallest) singularity exponent h_∞, which is well correlated with the evolution of the temperature anomaly associated with the upwelling $\delta T_{upwelling}$. Moreover, it has been observed that, for strong upwelling events, the strongest fronts are located close to the coast, while for weak upwelling events they can also be located offshore, confirming then, that the strongest fronts are generated by the upwelling process. The second main result is the existence of a linear correlation between the anomalous scaling of the structure functions measured by Δh^- and the most singular exponents h_∞. With the interpretation of singularity exponents as normalized measures of front intensity in mind, our results imply that anomalous scaling are linearly anti-correlated to the intensity of the strongest fronts. Putting these two results together, it implies that some statistical properties of the flow in the area under study, including the spectral slopes of SST, are correlated to the intensity of the upwelling.

An important question that emerges is whether the correlation and slope between h_∞ and Δh^- is universal. A preliminary answer would be positive for two main reasons: the same correlation between h_∞ and Δh^- has been found for different variables, SST and velocities; and it has been found in regions with different dynamical regimes, the California Current System and the Gulf stream (see Isern-Fontanet & Turiel, 2021). To confirm this answer it would be necessary to analyse global numerical simulations (Su et al., 2020) or observations (Merchant et al., 2019). However, before using SST measurements, it is necessary to address the problems generated by data gaps due to cloud coverage (Isern-Fontanet et al., 2021); the masking out of strong fronts by the failure of cloud mask algorithms (Kilpatrick et al., 2019); and the changes in Δh^- induced by noise (Isern-Fontanet & Hascoët, 2014). Among them, the most critical problem is the masking of strong fronts because it has a direct impact on the estimation of h_∞ and, thus, $\Delta h^- = h_d - h_\infty$. Besides, h_∞, Δh^- and the slope between them could be used to validate ocean models and compare models with data. These variables are, in principle, independent of the resolution and the algorithms for computing singularity exponents are robust (Pont et al., 2013).

6 Conclusions

Singularity exponents provide a measure of the intensity of SST fronts that can be connected to the scaling of the structure function and the spectral slope of SST through the singularity spectrum. When analysing the numerical simulations of the California Current System, results show that the intensity of the most singular fronts is correlated to the anomalous scaling of the structure functions. These fronts, at their turn, are closely related to the seasonal change of intensity of the coastal upwelling characteristic of this area. Our study points to the need to correctly reproduce the intensity of the strongest fronts and, consequently, properly model processes such as coastal upwelling in order to reproduce correctly SST statistics in ocean models.

7 Open Research

The details of the model configuration, as well as, the simulated Sea Surface Temperatures generated for this study and the singularity analysis described in Section 3 are available in https://doi.org/10.20350/digitalCSIC/14487 (Isern-Fontanet et al., 2022).

Acknowledgments

This work was supported by the Ministry of Economy and Competitiveness, Spain, and FEDER EU through the EXPLORA Ciencia National R+D Plan under TURBOMIX project (CGL2015-73100-EXP) and through the projects PROMISES (ESP2015-67549-C3-1-R) and COSMO (CTM2016-79474-R). This work was supported in part by the Spanish R&D project L-BAND (ESP2017-89463-C3-1-R), which is funded by MCIN/AEI/10.13039/501100011033 and ERDF A way of making Europee, and project INTERACT (PID2020-114623RB-C31), which is funded by MCIN/AEI/10.13039/501100011033. We also acknowledge support from Fundación General CSIC (Programa ComFuturo). This work acknowledges the 'Severo Ochoa Centre of Excellence' accreditation (CEX2019-000928-S). This work is a contribution to CSIC PTI Teledetect.

References

Arneodo, A., Bacry, E., & Muzy, J. F. (1995). The thermodynamics of fractals revisited with wavelets. *Physica A: Statistical Mechanics and its Applications*, *213*(1), 232–275. Retrieved from `https://www.sciencedirect.com/science/article/pii/037843719400163N` doi: https://doi.org/10.1016/0378-4371(94)00163-N

Callies, J., & Ferrari, R. (2013). Interpreting energy and tracer spectra of upper-ocean turbulence in the submesoscale range (1–200 km). *J. Phys. Oceanogr.*, *43*(11), 2456–2474. doi: 10.1175/JPO-D-13-063.1

Capet, X., Colas, F., Mcwilliams, J. C., Penven, P., & Marchesiello, P. (2008). Eddies in eastern boundary subtropical upwelling systems. In *Ocean modeling in an eddying regime* (p. 131-147). American Geophysical Union (AGU). Retrieved from `https://agupubs.onlinelibrary.wiley.com/doi/abs/10.1029/177GM10` doi: https://doi.org/10.1029/177GM10

Capet, X., McWilliams, J., Mokemaker, M., & Shchepetkin, A. (2008). Mesoscale to submesoscale transition in the california current system. Part I: Flow structure, eddy flux, and observational tests. *J. Phys. Oceanogr.*, *38*, 29–43.

Chang, Y., & Cornillon, P. (2015). A comparison of satellite-derived sea surface temperature fronts using two edge detection algorithms. *Deep Sea Research Part II: Topical Studies in Oceanography*, *119*, 40–47. Retrieved from `https://www.sciencedirect.com/science/article/pii/S0967064513004475` doi: https://doi.org/10.1016/j.dsr2.2013.12.001

Chenillat, F., Franks, P. J. S., Capet, X., Rivière, P., Grima, N., Blanke, B., & Combes, V. (2018). Eddy properties in the southern california current system. *Ocean Dynamics*, *68*(7), 761–777. Retrieved from `https://doi.org/10.1007/s10236-018-1158-4` doi: 10.1007/s10236-018-1158-4

D'Asaro, E., Lee, C., Rainville, L., Harcourt, R., & Thomas, L. (2011, 04). Enhanced turbulence and energy dissipation at ocean fronts. *Science*, *332*(6027), 318. Retrieved from `http://science.sciencemag.org/content/332/6027/318.abstract` doi: 10.1126/science.1201515

Deser, C., Alexander, M., Xie, S., & Phillips, A. (2010). Sea surface temperature variability: Patterns and mechanisms. *Annu. Rev. Mar. Sci*, *2*, 115–43. doi: 10.1146/annurev-marine-120408-151453

Frisch, U. (1995). *Turbulence: The legacy of A.N. Kolmogorov.* Cambridge MA: Cambridge Univ. Press.

Gulev, S., Thorne, P., Ahn, J., Dentener, F., Domingues, C., Gerland, S., ... R.S., V. (2021). Climate change 2021: The physical science basis. contribution of working group i to the sixth assessment report of the intergovernmental panel on climate change. In V. Masson- Delmotte et al. (Eds.), (chap. Changing State of the Climate System). Cambridge University Press.

Isern-Fontanet, J., García-Ladona, E., González-Haro, C., Turiel, A., Rosell-Fiechi, M., Company, J., & Padial, A. (2021). High resolution ocean currents from sea surface temperature observations: the catalan sea (western mediterranean). *Remote Sensing*, *13*, 3635. doi: 10.3390/rs13183635

Isern-Fontanet, J., Ballabrera-Poy, J., Turiel, A., & García-Ladona, E. (2017). Remote sensing of ocean surface currents: a review of what is being observed and what is being assimilated. *Nonlinear Processes in Geophysics*, *24*, 613 – 643. doi: 10.5194/npg-24-613-2017

Isern-Fontanet, J., Capet, X., Turiel, A., Olmedo, E., & González-Haro, C. (2022). *Simulated sea surface temperature and derived singularity exponents for the california current system (v.1.0) [dataset].* doi: https://doi.org/10.20350/digitalCSIC/14487

Isern-Fontanet, J., & Hascoët, E. (2014). Diagnosis of high resolution upper ocean dynamics from noisy sea surface temperature. *J. Geopys. Res.*, *118*, 1–12. doi: 10.1002/2013JC009176

Isern-Fontanet, J., Shinde, M., & González-Haro, C. (2014). On the transfer function between surface fields and the geostrophic stream function in the mediterranean sea. *J. Phys. Ocean*, *44*, 1406–1423. doi: 10.1175/JPO-D-13-0186.1

Isern-Fontanet, J., & Turiel, A. (2021). On the connection between intermittency and dissipation in ocean turbulence: A multifractal approach. *Journal of Physical Oceanography*, *51*(8), 2639–2653. Retrieved from https://journals.ametsoc.org/view/journals/phoc/51/8/JPO-D-20-0256.1.xml doi: 10.1175/JPO-D-20-0256.1

Isern-Fontanet, J., Turiel, A., García-Ladona, & Font, J. (2007). Microcanonical multifractal formalism: Application to the estimation of ocean surface velocities. *J. Geophys. Res.*, *112*, C05024. doi: 10.1029/2006JC003878

Ivanov, L. M., Collins, C. A., Marchesiello, P., & Margolina, T. M. (2009). On model validation for meso/submesoscale currents: Metrics and application to roms off central california. *Ocean Modelling*, *28*(4), 209–225. Retrieved from https://www.sciencedirect.com/science/article/pii/S1463500309000249 doi: https://doi.org/10.1016/j.ocemod.2009.02.003

Kilpatrick, K. A., Podestá, G., Williams, E., Walsh, S., & Minnett, P. J. (2019). Alternating decision trees for cloud masking in modis and viirs nasa sea surface temperature products. *Journal of Atmospheric and Oceanic Technology*, *36*(3), 387–407. Retrieved from https://journals.ametsoc.org/view/journals/atot/36/3/jtech-d-18-0103.1.xml doi: 10.1175/JTECH-D-18-0103.1

Kirches, G., Paperin, M., Klein, H., Brockmann, C., & Stelzer, K. (2016). Gradhist —a method for detection and analysis of oceanic fronts from remote sensing data. *Remote Sensing of Environment*, *181*, 264–280. Retrieved from https://www.sciencedirect.com/science/article/pii/S0034425716301584 doi: https://doi.org/10.1016/j.rse.2016.04.009

Mahadevan, A. (2016). The impact of submesoscale physics on primary productivity of plankton. *Annual Review of Marine Science*, *8*(1), 161-184. Retrieved from http://dx.doi.org/10.1146/annurev-marine-010814-015912 (PMID: 26394203) doi: 10.1146/annurev-marine-010814-015912

Merchant, C. J., Embury, O., Bulgin, C. E., Block, T., Corlett, G. K., Fiedler, E., ... Donlon, C. (2019). Satellite-based time-series of sea-surface temperature since 1981 for climate applications. *Scientific Data*, *6*(1), 223. Retrieved from https://doi.org/10.1038/s41597-019-0236-x doi: 10.1038/s41597-019-0236-x

Parisi, G., & Frisch, U. (1985). On the singularity structure of fully developed turbulence. In M. Ghil, R. Benzi, & G. Parisi (Eds.), *Turbulence and predictability* *in geophysical fluid dynamics. proc. intl. school of physics e. fermi* (p. 84-87). Amsterdam: North Holland.

Pont, O., Turiel, A., & Yahia, H. (2013, 08). Singularity analysis of digital signals through the evaluation of their unpredictable point manifold. *International Journal of Computer Mathematics*, *90*(8), 1693–1707. Retrieved from https://doi.org/10.1080/00207160.2012.748895 doi: 10.1080/00207160.2012.748895

Pope, S. B. (2000). *Turbulent flows.* Cambridge: Cambridge University Press. Retrieved from https://www.cambridge.org/core/books/turbulent-flows/C58EFF59AF9B81AE6CFAC9ED16486B3A doi: DOI:10.1017/CBO9780511840531

Shchepetkin, A., & McWilliams, J. (2005). The regional oceanic modeling system (roms): a split-explicit, free-surface, topography-following-coordinate oceanic model. *Ocean Modelling*, *9*(4), 347 – 404. Retrieved from http://www.sciencedirect.com/science/article/pii/S1463500304000484 doi: http://dx.doi.org/10.1016/j.ocemod.2004.08.002

Skákala, J., Cazenave, P. W., Smyth, T. J., & Torres, R. (2016, 2019/02/04). Using multifractals to evaluate oceanographic model skill. *Journal of Geophysical Research: Oceans*, *121*(8), 5487–5500. Retrieved from https://doi.org/10.1002/2016JC011741 doi: 10.1002/2016JC011741

Skákala, J., Smyth, T. J., Torres, R., Buckingham, C. E., Brearley, A., Hyder, P., & Coward, A. C. (2019, 2020/08/14). Sst dynamics at different scales: Evaluating the oceanographic model resolution skill to represent sst processes in the southern ocean. *Journal of Geophysical Research: Oceans*, *124*(4), 2546–2570. Retrieved from https://doi.org/10.1029/2018JC014791 doi: 10.1029/2018JC014791

Su, Z., Torres, H., Klein, P., Thompson, A. F., Siegelman, L., Wang, J., … Hill, C. (2020, 2021/03/03). High-frequency submesoscale motions enhance the upward vertical heat transport in the global ocean. *Journal of Geophysical Research: Oceans*, *125*(9), e2020JC016544. Retrieved from https://doi.org/10.1029/2020JC016544 doi: https://doi.org/10.1029/2020JC016544

Sukhatme, J., Chaudhuri, D., MacKinnon, J., Shivaprasad, S., & Sengupta, D. (2020, 07). Near-Surface Ocean Kinetic Energy Spectra and Small-Scale Intermittency from Ship-Based ADCP Data in the Bay of Bengal. *Journal of Physical Oceanography*, *50*(7), 2037–2052. Retrieved from https://doi.org/10.1175/JPO-D-20-0065.1 doi: 10.1175/JPO-D-20-0065.1

Turiel, A., Pérez-Vicente, C. J., & Grazzini, J. (2006). Numerical methods for the estimation of multifractal singularity spectra on sampled data: A comparative study. *Journal of Computational Physics*, *216*(1), 362–390. Retrieved from http://www.sciencedirect.com/science/article/pii/S0021999105005565 doi: https://doi.org/10.1016/j.jcp.2005.12.004

Turiel, A., Yahia, H., & Pérez-Vicente, C. J. (2008). Microcanonical multifractal formalism—a geometrical approach to multifractal systems: Part I. Singularity analysis. *Journal of Physics A: Mathematical and Theoretical*, *41*(1), 015501. Retrieved from http://dx.doi.org/10.1088/1751-8113/41/1/015501 doi: 10.1088/1751-8113/41/1/015501

Yu, K., Dong, C., & King, G. P. (2017, 2021/10/04). Turbulent kinetic energy of the ocean winds over the kuroshio extension from quikscat winds (1999–2009) [https://doi.org/10.1002/2016JC012404]. *Journal of Geophysical Research: Oceans*, *122*(6), 4482–4499. Retrieved from https://doi.org/10.1002/2016JC012404 doi: https://doi.org/10.1002/2016JC012404